OPEN ACCESS
Journal of Multidisciplinary Applied Natural Science Vol. xx No. xx (xxxx) https://doi.org/10.47352/jmans.2774-3047.459
Check for updates
Research Article

Waste-derived CaO Modified TiO_2 with Reduced Band Gap and Improved Photoresponse under Visible Light

Siti Rodiah*, Ratih Rizqi Nirwana, Desti Erviana, Nina Ariesta, Damayanti Iskandar, and Hapin Afriyani

Received : January 7, 2026	Revised : May 4, 2026	Accepted : May 21, 2026	Online : July 22, 2026

Abstract
Titanium dioxide (TiO_2) is the most extensively investigated photocatalysts, but its high band gap energy limits its photoactivity primarily to the ultraviolet region. This study presents a green approach to enhanced visible-light absorption of TiO_2 by utilizing calcined golden snail shells as a sustainable and low-cost precursor for CaO dopant. The TiO_2-CaO composites were synthesized via a simple loading technique. Characterization confirmed the successful distribution of CaO onto the TiO_2 surface, reducing in the band gap energy of TiO_2 from 3.334 eV to 3.322 eV. This modification substantially broadened the material's light absorption into the visible spectrum. The optimized composites demonstrated feasible photocatalytic activity for the reduction of CO_2 under simulated solar irradiation with the addition of *Clitoria ternatea* photosensitizer, achieving initial activity higher than that of pure TiO_2. This work successfully combines the waste-derived CaO, offering a promising, environmentally friendly, and highly effective green material to improved photoresponse under visible light of TiO_2.

Keywords: band gap energy; golden snail shells-derived CaO; TiO_2-CaO composite; visible light absorption

1. INTRODUCTION

Photochemical reactions, which are driven by light energy, necessitate the use of semiconductor materials with specific properties. The remarkable characteristics of TiO_2 in many electrochemical processes have been extensively examined. TiO_2 is capable of facilitating electrochemical reactions even without the application of an external voltage [1]. Prior research has characterized n-type TiO_2 as a photo-assistance agent, denoting a material that not only absorbs light energy but also efficiently directs that energy into the intended reaction pathways. When doped with tungsten, n-type TiO_2 shows a significant response close to its band gap energy (Eg ~3.0 eV), which corresponds to wavelengths of around 350 nm. This response can shift by up to 0.5 eV toward the blue region (visible light) [2]. Anatase TiO_2 crystals exhibit a Eg of 3.2 eV when produced using reactive magnetron sputtering [3] and are generally amorphous with minimal crystallite dimensions. Doping TiO_2 facilitates a decrease in band gap energy, thereby broadening its photoactivity into the visible light spectrum.

Numerous supporting materials have been used as supports for TiO_2, including Cu, Ag, MWCNT, Ag–MWCNT, CNT@Ni, UiO-66, Rh, Ru, Pt, and Zn, all of which were synthesized in different ways [4]-[7]. Previous research indicates that metal oxides (MO) have been less frequently employed to modify TiO_2 in comparison to metal doping, which continues to be the most prevalent modification method. One notably intriguing dopant is calcium, incorporated via calcium nitrate and synthesized as nanoparticles (Ca–TiO_2 NPs). Ca doping has been demonstrated to decrease the Eg of pure TiO_2, thereby shifting its light absorption from ultraviolet to visible radiation [8]. This phenomenon is attributed to introduction of additional electrons by calcium, which generates new energy states within the band structure [8]. In addition, modification with MO can improve charge carrier separation through the formation of heterojunctions between the oxide phase and TiO_2, effectively promoting spatial separation of redox processes while suppressing charge recombination and competing side reaction [9]. Consequently, the incorporation of calcium oxide (CaO) offers a promising approach for Eg engineering in TiO_2. The abundant availability of CaO further enhances its potential as

Please cite this article as: S. Rodiah, R. R. Nirwana, D. Erviana, N. Ariesta, D. Iskandar, and H. Afriyani. (2026). "Waste-derived CaO Modified TiO_2 with Reduced Band Gap and Improved Photoresponse under Visible Light". *Journal of Multidisciplinary Applied Natural Science*. https://doi.org/10.47352/jmans.2774-3047.459

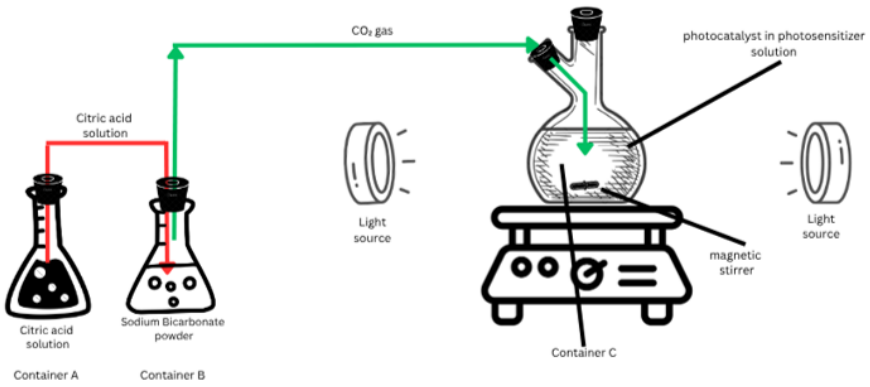

Figure 1. Schematic illustration of the reactor used for CO_2 photoreduction over CaO-doped TiO_2 under light irradiation in the presence of *Clitoria ternatea* as a photosensitizer.

a cost-effective support material. Although TiO_2 doping with various materials has been thoroughly investigated, the utilization of natural waste as a sustainable source of dopant materials remains an area of further research.

Golden snail shells have been shown to contain 61.95% CaO during calcination at 800 °C [10], indicating their viability as a sustainable source of CaO. The CaO serves as a promising dopant semiconductor material and has exhibited superior efficacy as a support for $MnFe_2O_4$ in the photodegradation of methylene blue [11]. Moreover, prior research has demonstrated that the particle size of CaO can be customized; for instance, CaO NPs have been effectively synthesized via a co-precipitation approach [12]. Nevertheless, the associated changes in Eg have not yet been comprehensively investigated. Previous studies have reported that the incorporation of calcium into TiO_2 as a dopant can modify the crystal structure of TiO_2 through the formation of crystal defects [8] and oxygen vacancies [9]. In the present study, CaO derived from golden snail shell waste was incorporated into TiO_2, and its effect on the reduction of Eg energy was evaluated. Phase structure, crystallite size, specific surface area, and pore structure are important factors influencing TiO_2 performance, all of which may be affected using raw materials with different compositions. Therefore, current study addressed the complete procedure, from the fabrication of the dopant source obtained from natural waste to its role in reducing the band gap in TiO_2. The visible-light activity of TiO_2 had been evaluated using CO_2 photoreduction generated by the reaction between sodium bicarbonate and citric acid in alkaline conditions. *Clitoria ternatea* photosensitizer was added to facilitate adequate absorption of visible light photons because TiO_2 is an indirect Eg semiconductor, where electrons released from the valence band during the excitation process experience momentum before being transferred to the conduction band. The photocatalyst's physicochemical properties were investigated by FT-IR, UV–Vis DRS, XRD, SEM, and BET analyses.

2. MATERIALS AND METHODS

2.1. Materials

Golden snail shells (*Pomacea canaliculate*) were collected from rice fields in Palembang and utilized as a source of CaO, prepared via the calcination method without further purification. TiO_2, polyethylene glycol (PEG6000), citric acid, sodium bicarbonate were purchased from Merck (analytical grade) and used as received. Distilled water and filter paper were purchased from Bratachem. *Clitoria ternatea* flowers as prepared as photosensitizer.

2.2. Methods

2.2.1. Preparation of CaO from Golden Snail Shells

CaO was prepared from golden snail shells using a slightly modified version of the process previously used by researchers [13]. After removing the golden snail shells from the leftover meat with flowing water, the shells were crushed and calcined

for two hours at 900 °C to produce shell powder. A Bruker Alpha FT-IR-ATR fitted with diamond crystals was used to evaluate the shell powder to detect the presence of CaO functional groups.

2.2.2. Preparation of Photocatalyst TiO_2-CaO

TiO_2-CaO photocatalyst was made by co-precipitation method by mixing TiO_2 powder, CaO, and PEG6000 in a 2:1:1 (w/w) ratio with 40 mL of distilled water for 1 h at 350 rpm. The precipitate was dried for 20 min at 70 °C. A Bruker Alpha FT-IR-ATR, UV Vis DR, and XRD were used to investigate the TiO_2-CaO photocatalyst properties.

2.2.3. Photoreduction of CO_2 to Methanol

The CO_2 photoreduction reactor scheme in this study was a modified version of the scheme reported by Jenny et al.[14]. Photoreduction begins with the preparation of the necessary reactants. The *C. ternatea* flowers were washed with water, dried, then crushed to produce butterfly pea flower powder. Carbon dioxide gas was generated from the reaction between 1.92 g of citric acid dissolved in 100 mL of distilled water contained in container A and 2.52 g of sodium bicarbonate in container B. Both containers were linked by two hoses; the first hose was designated for transferring the citric acid solution from container A to container B, while the second hose was used to convey CO_2 gas from container B to container C, which contains 1 g of photocatalyst and a butterfly pea flower solution (comprising 1 g of butterfly pea flower powder dissolved in 100 mL of distilled water). The photocatalyst and photosensitizer were put into a photoreactor equipped with a light source as indicated in Figure 1.

2.2.4. Characterization

In this study, the instruments were used to characterize the properties of photocatalyst and to analyse the product obtained. FT-IR spectra were recorded using a Bruker Alpha FT-IR (Bruker optics, Germany) in ATR mode over 4000–500 cm^{-1} at a resolution of 4 cm^{-1}. UV-Vis diffuse reflectance spectra were measured in the range of 200–800 nm using $BaSO_4$ as reference and analyzed via the Kubelka-Munk function. XRD patterns were obtained using a diffractometer with Cu Kα radiation (λ=1.5406 Å), operated at 40 kV and 30 mA over a 2θ range of 10–90°. SEM-EDX analysis was performed using a Zeiss scanning electron microscopes (SEM, Germany) equipped with an EDX detector. The instruments was operated at an accelerating voltage of 10–15 kV. The samples were gold-coated prior to imaging and elemental composition was analyzed using EDX. Methanol analysis was performed using GC-MS equipped with a polar capillary column and helium as the carrier gas (1.0 mL/min). The oven temperature was programmed from 40 °C (held for 3 min) and increased at 5 °C/min to 230 °C, with the injector set at 230 °C and a split ratio of 20:1.

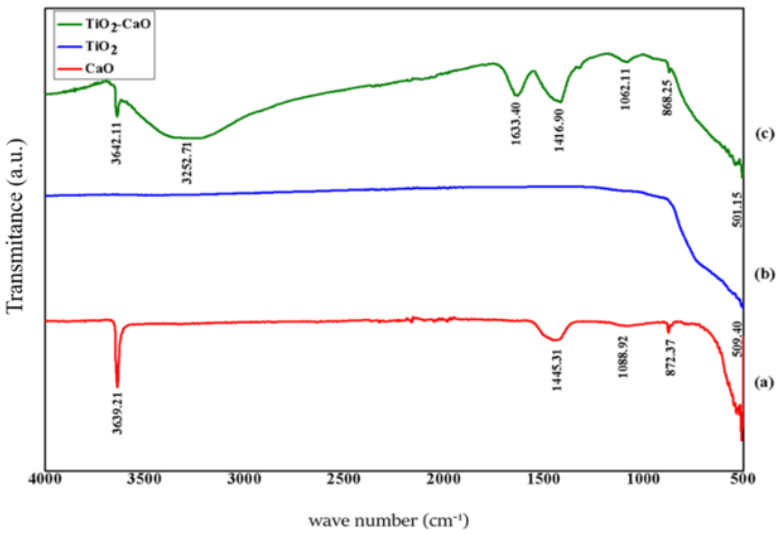

Figure 2. FTIR spectra of (a) CaO from golden snail shell waste; (b) pure TiO_2; and (c) synthesized TiO_2-CaO.

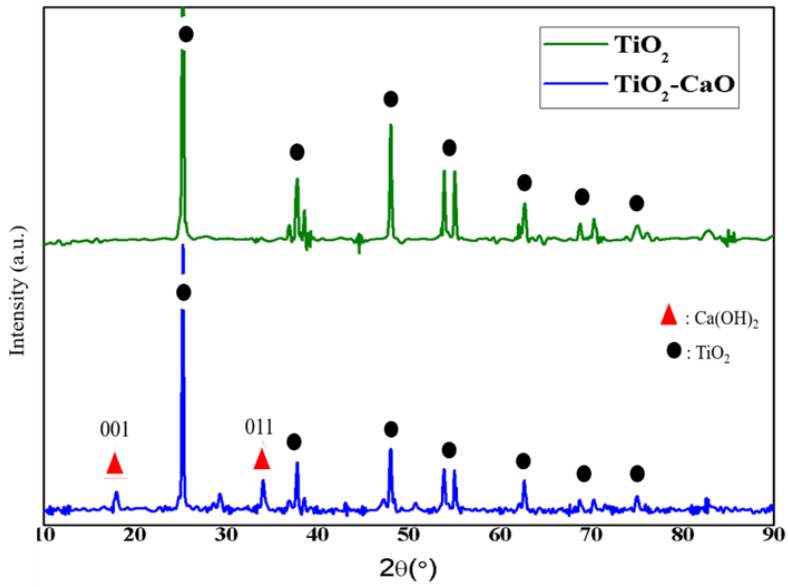

Figure 3. XRD patterns of pure TiO_2 and TiO_2-CaO synthesized samples confirm the presence of anatase TiO_2, while the addition of CaO is associated with a reduction of crystallinity.

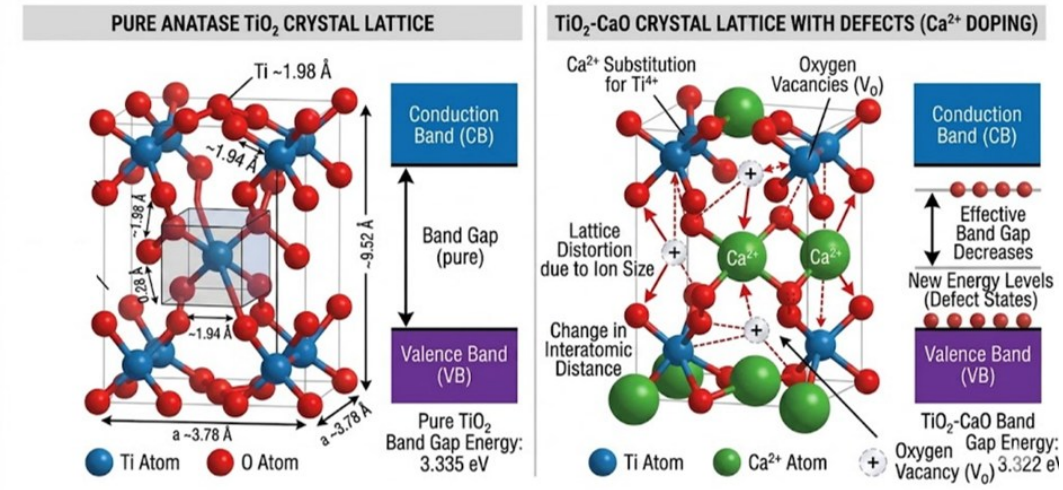

Figure 4. Schematic representation of defect and oxygen vacancy formation in CaO-doped TiO_2 and its effect on band gap energy reduction.

Detection was carried out using electron impact ionization (70 eV) over an m/z range 40-500, and quantification was based on an internal standard using peak area ratios.

3. RESULTS AND DISCUSSIONS

3.1. Preparation of photocatalyst TiO_2-CaO

The TiO_2-CaO photocatalyst in this study was produced from TiO_2 and CaO derived from golden snail shells through the co-precipitation process by adding PEG6000. CaO was obtained after golden snail shells was decomposed during calcination at 900 °C for 2 h by releasing CO_2 gas as shown in Equation (1). Prior research indicated that the conversion of $CaCO_3$ to CaO was accomplished at 800 °C, therefore, calcination at 900°C for two hours was adequate to convert $CaCO_3$ to CaO [12]. PEG6000 serves as a carrier for TiO_2 and CaO, thereby minimizing the possibility of agglomeration. TiO_2-CaO will coat the surface of PEG6000, enhancing its photocatalytic performance [16][19].

$$CaCO_{3(s)} \rightarrow CaO_{(s)} + CO_{2(g)} \quad \textbf{(1)}$$

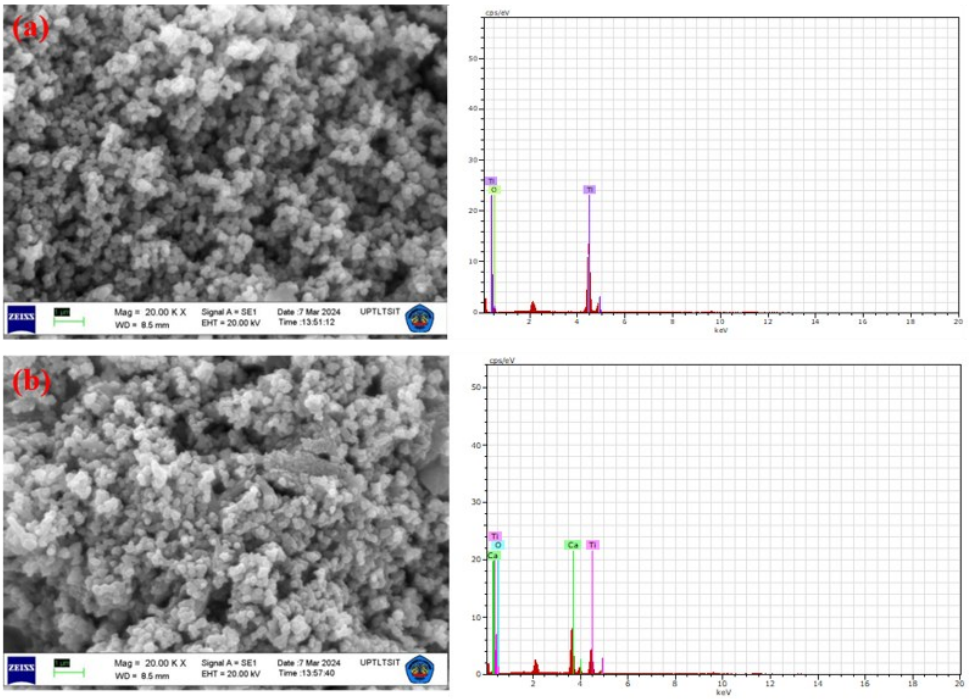

Figure 5. SEM-EDX images of (a) pure TiO_2 and (b) TiO_2-CaO synthesized samples at 20,000× magnification, demonstrating predominantly spherical morphology with increased pore size in the TiO_2-CaO sample.

Table 1. BET adsorption-desorption isotherm and BJH pore size distribution curves of pure TiO_2 and TiO_2-CaO synthesized samples.

Parameter	TiO_2	TiO_2.CaO
Surface Area (m^2/g), BET	7.39997	2.4849
Pore Size (nm), BJH	4.51039	8.57078
Pore Volume (cm^3/g), BJH	0.0166884	0.0106488

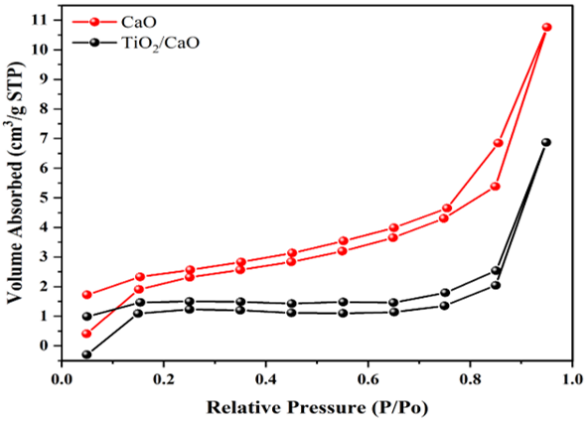

Figure 6. The N_2 isotherm and pore size distribution of CaO and TiO_2-CaO synthesized samples.

Table 2. Elemental Composition in pure TiO_2 and TiO_2-CaO synthesized samples.

Element	TiO_2	TiO_2-CaO
Ti	41.47%	15.56%
O	58.53%	63.99%
Ca	-	20.46%

3.2. FT-IR Analysis

Functional group analysis was carried out using an FT-IR instrument to confirm that CaO had successfully attached to the surface of TiO_2. The existence of CaO from golden snail shells and TiO_2 in TiO_2-CaO synthesized was verified by comparing the FT-IR spectra of TiO_2, CaO, and TiO_2-CaO in Figure 2.

The TiO_2 spectra (Figure 2(b)) in the current study appeared clearly at a wavenumber of 509 cm^{-1}, which corresponds to the stretching vibration of Ti–O and Ti–O–Ti. This vibration observed at 501 cm^{-1} in TiO_2-CaO spectra (Figure 2(c)). Concurrently, the FT-IR spectrum in Figure 2(a) shows several characteristic peaks indicating the presence of calcium oxide phase and its derivative products. The weak band observed at 500–700 cm^{-1} are attributed to Ca–O vibrational mode [15][16] indicating the presence of CaO. However, the appearance of a sharp peak at 3639 cm^{-1} indicates the presence of hydroxyl (O–H) groups, which are associated with the formation of calcium hydroxide due to the hydration of CaO [15] - [17] as described in Equation (2).

$$CaO_{(s)} + H_2O_{(l)} \rightarrow Ca(OH)_{2(s)} \quad (2)$$

Additionally, the peak observed at 872, 1089, and 1445 cm^{-1} correspond to the bending and stretching vibrations of carbonate (CO_3^{2-}) groups, respectively. These features suggest that part of the CaO has undergone carbonation through chemisorption of atmospheric CO_2 on the catalyst surface (see Equation (3)) [8][9][18][19].

$$CaO_{(s)} + CO_{2(g)} \rightarrow CaCO_{3(s)} \quad (3)$$

Meanwhile, the presence of OH group at the TiO_2-CaO spectra (Figure 2(c)) showed the appearance of two sharp and broad absorptions at wavenumbers of 3642 and 3253 cm^{-1}. The region of the IR spectra at wavenumbers >3300 cm^{-1} is the region completely dominated by the stretching vibration of the OH group, which is usually involved in the hydrogen bonding network of the crystal [20]. The success of CaO as a support and bonding with TiO_2 in the synthesized photocatalyst was shown by the appearance of new absorption from $CaTiO_3$ at 1062 cm^{-1} and was confirmed by the presence of Ti–O vibrations at 501 cm^{-1} [21] [22].

3.3. XRD Analysis

The crystal phase was confirmed by comparing the TiO_2 and TiO_2-CaO diffractogram patterns shown in Figure 3. The XRD patterns of TiO_2 and TiO_2-CaO exhibit similar diffraction peaks, indicating the preservation of the TiO_2 crystalline structure after CaO addition. Characteristic peaks of TiO_2 are observed at 2θ = 25.28°, 37–38°, 48°, 53–55°, 62–63°, 70°, 75°, and 82–83°, which are attributed to the anatase phase and are consistent with COD card no. 7206075. The dominant peak at 2θ = 25.28° confirms the presence of anatase TiO_2. Furthermore, the presence of CaO in TiO_2-CaO enables its reaction with H_2O to form $Ca(OH)_2$ with

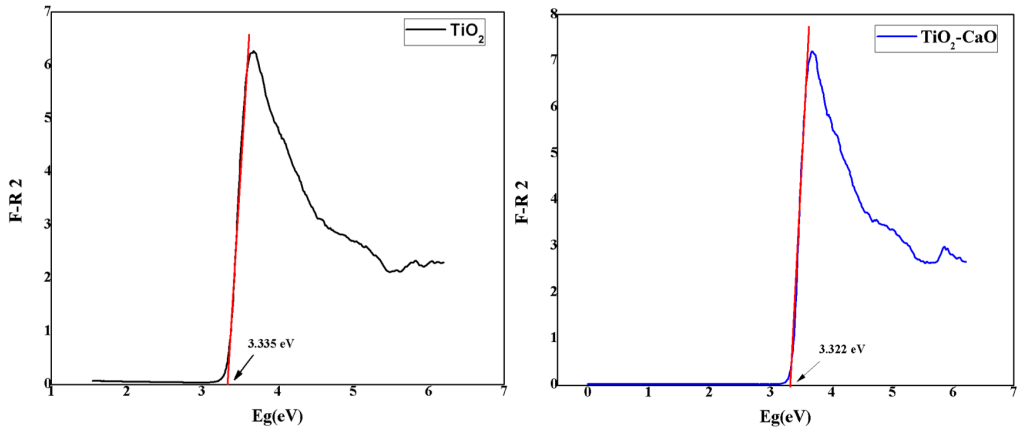

(a) (b)

Figure 7. UV Vis-DRs spectra of (a) pure TiO_2 and (b) TiO_2-CaO synthesized samples.

Table 3. Identification and characterization of compounds generated via photocatalytic reactions employing TiO_2 and TiO_2–CaO catalysts under visible and UV irradiation, as determined by GC–MS analysis.

Interpretation of compounds	Retention Time (min)	Base Peak (m/z)	Peak Area (%)	Catalyst	Light source
Aliphatic amine (2-amino-6-methylheptane or Octodrine)	1.389	44	21.45	TiO_2	Visible
	1.700		53.17		
	2.350		25.38		
Bicyclo [2.2.1] heptane,-5-(ethyl -1-amine) and DL-α-Alanine	1.688	44	96.92		UV
	2.440		3.08		
Bicyclo[2.2.1] heptane,-5-(ethyl-1-amine)	1.696	44	90.96		Visible
	2.114		1.15		
	3.036		7.89		
Bicyclo[2.2.1] heptane,-5-(ethyl-1-amine) and 5-methyl-2-Heptanamine,	1.724	44	53.68	TiO_2–CaO	UV
	2.005		2.34		
	3.054		2.35		
	3.494		41.63		

characteristic peaks at 2θ of 18.04° and 34.06° [23], corresponding to the (001) and (011) planes, respectively consistent with COD card no. 1001768.

Based on peak sharpness, the two diffractogram do not show a significant difference. However, the peak intensity of TiO_2 is higher than TiO_2-CaO, indicating a decrease in the crystallinity of TiO_2 after the addition of CaO. The characteristic peak of the anatase TiO_2 phase appear in both diffractogram with slight chemical shift, meanwhile in the TiO_2-CaO XRD pattern, these peaks are more dominant. The presence of CaO inhibits lattice re-organization associated with the transformation from anatase to rutile, thereby stabilizing the anatase phase and prolonging its retention in a less ordered nanocrystalline structure [24]. In addition, the formation of a new phase, $CaTiO_3$ (confirmed by FT-IR spectra) at elevated temperatures reduce the TiO_2 fraction, leading to decrease crystallinity [25]. Furthermore, the incorporation of CaO also affects the band gap energy. The incorporation of Ca^{2+} ions into the TiO_2 crystal lattice induces structural defects, including lattice distortion and oxygen vacancies (as illustrated at Figure 4). These defects introduce new energy levels below the conduction band of TiO_2. Electron associated with Ca^{2+} can occupy these levels and require lower excitation energy [8][9][18] resulting in reduction of the effective Eg as confirmed by UV-DRS results.

3.4. SEM-EDX, BET and BJH Analysis

Confirmation of the successful modification of TiO_2 with CaO from golden snail shells in terms of morphology using SEM-EDX analysis is shown in Figure 5, combined with BET and BJH analysis methods as depicted in Figure 6. Figure 5 shows that the uniformly spherical TiO_2 morphology [8] has a larger specific surface area than TiO_2-CaO (see Table 1). The incorporation of CaO on the TiO_2 surface results in a threefold reduction in specific surface area and a 1.5-fold decrease in pore volume, accompanied by an approximately twofold increase in pore size. Thus, the presence of CaO results in the TiO_2 pores becoming wide and shallow. Additionally, the pore size distribution of CaO plays a crucial role in determining the pore size uniformity of the synthesized TiO_2–CaO (Figure 6).

In contrast, CaO-modified TiO_2 exhibited a relatively larger and more spherical morphology than pure TiO_2. The SEM results indicate that TiO_2-CaO has a particles size of 25 nm, compared to 12 nm for TiO_2. Previous studies have reported that the co-precipitation method may lead to particle agglomeration [26][27]. As discussed previously, the use of PEG6000 as a capping agent to link TiO_2 with CaO during the synthesis process reduces the possibility of agglomeration [21][28]. Meanwhile, in this work, agglomerates were seen to form in

various locations due to small spherical TiO_2 adhering to CaO, which had an irregular shape and a bigger size. Additionally, the elemental content of the TiO_2-CaO photocatalyst (Table 2) revealed that Ca is more dominant than Ti since the Ca element is higher than Ti.

3.5. UV Vis-DRS Analysis

TiO_2 is a semiconductor with a broad Eg in the range of 3.20–3.56 eV [29] that forms in three crystal phases: anatase, rutile, and brookite. Anatase and rutile exhibit tetragonal crystal structures, whereas brookite show an orthorhombic crystal structure. Due to its higher electron mobility, anatase is the more favorable of the three phases as a photocatalyst [8]. According to the UV Vis-DRs spectra in Figure 7, TiO_2 and TiO_2-CaO had band gap energies of 3.335 and 3.322 eV respectively, indicating that the CaO support on TiO_2 reduced the band gap energy by 0.013 eV. Additional energy from CaO between TiO_2's valence and conduction bands narrow the electron excitation distance and shifts the edge wavelength toward visible light [30]. Consequently, the synthesized TiO_2-CaO photocatalyst exhibits enhanced photocatalytic activity in the visible light spectrum when compared to TiO_2. This is supported by the study's findings, loading CaO to TiO_2 decreased the energy band gap causes this material to be active in visible light spectrum.

3.6. Photoreduction of CO_2 to Methanol

In this study, CO_2 gas used is the result of the reaction between citric acid solution and sodium bicarbonate (see Equation (4)). The CO_2 gas was subsequently reduced using TiO_2 and TiO_2-CaO catalysts. The reaction performance in the visible and ultraviolet light regions was examined to observe the catalyst activity in specific light regions.

$$H_3C_6H_5O_{7(aq)} + 3NaHCO_{3(s)} \rightarrow Na_3C_6H_5O_{7(aq)} + 3H_2O_{(l)} + 3CO_{2(g)} \quad \textbf{(4)}$$

Gaseous products like CO, CH_4, and ethylene (C_2H_4) were frequently produced by CO_2 reduction and were easily identified along with byproducts like H_2, O_2, and N_2 from leaks [31]. Gaseous products from CO_2 photoreduction were analyzed using gas chromatography (GC) by comparing retention periods to calibrated gas standards under the same chromatographic circumstances (e.g., CO_2, CO, CH_4), each compound was identified as shown in Table 3.

According to the results of the MS analysis, this data indicates a greater diversity in product variations. The primary peak, which has a dominant area percentage, exhibits at a retention time of 1.6–1.8 min and has an area percentage from 50–97%. The most prominent feature of this peak is the m/z 44 fragment, which is the most prominent characteristic. Although methanol is not produced, the compound that is generated has an amine group and an amino acid (alanine), which is a very unexpected but reasonable result. Table 4 presents several possibilities for m/z 44 fragments, which include indicating the existence of an amine attributed to the nitrogen constituent of secondary metabolites, primarily anthocyanins, present in the *C. ternatea* extract utilized as a photosensitizer. The synthesized catalyst transforms CO_2 into an oxygenate intermediate or generates acetaldehyde. The system retains residual CO_2 that is not fully reduced, resulting in peak 44 manifesting as the parent molecule. The amino acid alanine is created by a complicated interaction between CO_2 and nitrogen molecules. The m/z 44 fragment is generated via decarboxylation, or the breakage of

Table 4. Proposed structural assignments for the prominent m/z 44 base peak based on electron ionization (EI) fragmentation patterns of amines, carboxylic acids, and CO_2.

Source Compound	Parent Molecular Structure	Fragment Structure (m/z 44)
Aliphatic amines	$R\text{-}CH(NH_2)CH_3$	$[CH_3\text{-}CH{=}NH_2]^+$
Carbon dioxide	$O{=}C{=}O$	$[O{=}C{=}O]^{+\circ}$
Ethanal (acetaldehyde)	CH_3CHO	$[CH_2{=}CH\text{-}OH]^{+\circ}$
DL-Alanine (amino acid)	$CH_3CH(NH_2)COOH$	$[CH_3\text{-}CH{=}NH_2]^+$

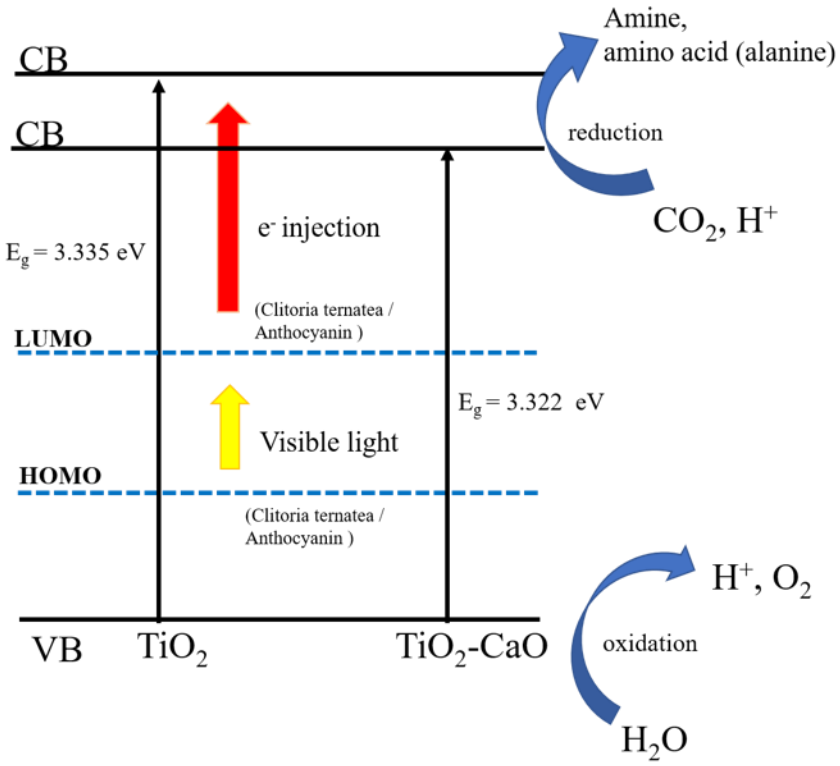

Figure 8. TiO_2 and TiO_2–CaO band gap diagrams and their implications for increasing photocatalytic activity under light irradiation.

the carbon-carbon bond, resulting in the release of a charged amino group. This fragment may also derive from free amino acids present in the extract of the *C. ternatea* plant.

This study evaluated the performance of TiO_2 and TiO_2-CaO in CO_2 reduction under visible and UV light. Figure 8 depicts the reduction in TiO_2's band gap energy both before and after CaO doping, along with the implications for enhancing photocatalytic activity when exposed to visible light. TiO_2 exposed to UV light generated a dominant peak product with a larger percentage area than TiO_2 exposed to visible light, which was 96.92%, as shown in Table 3. However, the TiO_2-CaO catalyst working under visible light yielded more dominant products, 90.96%. This suggests that the decrease in band gap that occurs as a result of doping with CaO has an effect on the characteristics of TiO_2 as well as its catalytic sensitivity towards visible light.

4. CONCLUSIONS

This study successfully implemented the modification of TiO_2 photocatalyst using CaO support derived from golden snail shells obtaining the anatase crystal phase. Synthesized TiO_2-CaO has a smaller specific surface area, greater pore size, uniform pore size distribution, and a larger spherical shape than TiO_2. The current work also demonstrates that catalyst modification and irradiation wavelength significantly influence the photocatalytic performance of TiO_2-based catalysts in CO_2 reduction. The introduction of CaO into TiO_2 effectively decreased the band gap energy from 3.334 eV to 3.322 eV, thereby improving activity under visible light irradiation. GC–MS analysis identified a predominant m/z 44 fragment with retention periods of 1.6–1.8 min, associated with nitrogenous organic substances, such as aliphatic amines and amino acids. The manufacturing of these compounds, instead of methanol or basic hydrocarbons, is credited to the interaction between CO_2 and nitrogen-based secondary metabolites, particularly anthocyanins from *Clitoria ternatea* extract performing as a photosensitizer. Under mild irradiation conditions, the enhanced visible-light responsiveness of TiO_2–CaO and the observed product diversity show that combining natural photosensitizers with catalyst

modification to encourage different CO_2 reduction techniques is feasible.

AUTHOR INFORMATION

Corresponding Author

Siti Rodiah — Department of Chemistry, Universitas Islam Negeri Raden Fatah Palembang, Palembang-30267 (Indonesia);
orcid.org/0000-0002-8132-2719
Email: siti.rodiah_uin@radenfatah.ac.id

Authors

Ratih Rizqi Nirwana — Department of Chemistry, Universitas Islam Negeri Walisongo, Semarang 50216 (Indonesia);
orcid.org/0000-0002-0302-3860

Desti Erviana — Department of Chemistry, Universitas Islam Negeri Raden Fatah Palembang, Palembang-30267 (Indonesia);
orcid.org/0009-0007-5431-3239

Nina Ariesta — Department of Chemistry, Universitas Nusa Bangsa, Bogor 16166 (Indonesia);
orcid.org/0000-0003-3772-9666

Damayanti Iskandar — Department of Chemistry, Universitas Islam Negeri Raden Fatah Palembang, Palembang-30267 (Indonesia); Departement Biomaterial, Okayama University, Okayama-7008530 (Japan);
orcid.org/0000-0001-8287-1579

Hapin Afriyani — Department of Chemistry, Lampung University, Bandar Lampung-35141 (Indonesia);
orcid.org/0000-0002-6092-127X

Author Contributions

This research was designed and supervised by S. R., while the conducting of the laboratory experiment was done by D. E. All authors contributed to the preparation of manuscript. The first draft of the manuscript was written by D. E. then critically reviewed by S. R., R. R., N, N. A., D. I., and H. A. The final version of the manuscript was refined S. R.

Conflicts of Interest

The authors declare no conflict of interest.

ACKNOWLEDGEMENT

This research was funded by DIPA UIN Raden Fatah Palembang based on SK Rector Number 748 Year 2023. The funding was administered through the Institute for Research and Community Service (LP2M UIN Raden Fatah Palembang).

DECLARATION OF GENERATIVE AI

Not applicable.

REFERENCES

[1] A. Fujishima, X. Zhang, and D. A. Tryk. (2007). "Heterogeneous Photocatalysis: From Water Photolysis to Applications in Environmental Cleanup". *International Journal of Hydrogen Energy*. **32** (14): 2664–2672. 10.1016/j.ijhydene.2006.09.009.

[2] M. S. Wrighton, D. S. Ginley, P. T. Wolczanski, A. B. Ellis, D. L. Morse, and A. Linz. (1975). "Photoassisted Electrolysis of Water by Irradiation of a Titanium Dioxide Electrode". *Proceedings of the National Academy of Sciences of the United States of America*. **72** (4): 1518–1522. 10.1073/pnas.72.4.1518.

[3] C. Guillén. (2025). "Band Gap Energy and Lattice Distortion in Anatase TiO2 Thin Films Prepared by Reactive Sputtering with Different Thicknesses". *Materials*. **18** (10): 10.3390/ma18102346.

[4] Z. U. Rehman, M. Bilal, J. Hou, F. K. Butt, J. Ahmad, S. Ali, and A. Hussain. (2022). "Photocatalytic CO2 Reduction Using TiO2-Based Photocatalysts and TiO2 Z-Scheme Heterojunction Composites: A Review". *Molecules*. **27** (7): 2069. 10.3390/molecules27072069.

[5] S. R. Firoozabadi, M. R. Khosravi-Nikou, and A. Shariati. (2023). "CO2 Photoreduction Using TiO2 Nanoflower/UiO-66 Composite Under UV Light Irradiation". *Journal of Environmental Chemical Engineering*. **11** (5): 110978. 10.1016/j.jece.2023.110978.

[6] M. Yadav, H. S. Basheer, and B. Abrah. (2023). "Noble Metals-Deposited TiO2 Photocatalysts for Photoreduction of CO2:

Exploration of Surface Chemistry and a Reflection on the Importance of Wavelength Dependence". *Applied Catalysis A: General*. **668** : 119434. 10.1016/j.apcata.2023.119434.

[7] N. A. Y. Abduh, T. S. Algarni, and A. B. Al-Odayni. (2025). "Green Synthesis of Zn-Doped TiO2 Nanomaterials for Photocatalytic Degradation of Crystal Violet and Methylene Blue Dyes Under Sunlight". *Biomass Conversion and Biorefinery*. **15** (3): 4849–4865. 10.1007/s13399-024-06120-0.

[8] Y. Etafa, T. Kumar, R. Krishnaraj, and S. Sarma. (2024). "Band Gap Engineering of Titanium Dioxide (TiO2) Nanoparticles Prepared via Green Route and Its Visible Light Driven for Environmental Remediation". *Results in Chemistry*. **11** : 101850. 10.1016/j.rechem.2024.101850.

[9] Y. E. Tasisa and M. G. R. Krishnaraj. (2025). "Green Synthesis of Ca/Sr Co-Doped TiO2 Nanoparticles: Impact on Morphology, Band Gap Reduction, Supercapacitor, and Visible-Light Photocatalytic Efficiency". *Discover Applied Sciences*. **7** : 979. 10.1007/s42452-025-06976-5.

[10] F. Rahman and S. Rodiah. (2020). "The Effect of CaO Catalyst Mass from Golden Snail Shell (Pomacea canaliculata) on Transesterification Reaction". *Alkimia: Jurnal Ilmu Kimia dan Terapan*. **4** (2): 88–92. 10.19109/alkimia.v4i2.8084.

[11] S. Rodiah and E. Ramadhani. (2022). "Highly Efficient Removal of Methylene Blue Dye from Wastewater Using CaO-MnFe2O4 Nanoparticles Prepared with Teak Leaf Extract". Al-*Kimia: Jurnal Ilmu Kimia dan Terapan*. **9** (2): 62–67. 10.15575/ak.v9i2.20068.

[12] N. Razali, F. Musa, N. Jumadi, and A. Jalani. (2021). "Production of Calcium Oxide from Eggshell: Study on Calcination Temperature, Raw Weight and Contact Time". *the Proceedings of the RSU International Research Conference*.

[13] S. Rodiah, D. Erviana, F. Rahman, and A. W. Budaya. (2020). "Modified CaO Catalyst from Golden Snail Shell (Pomacea canaliculata) for Transesterification Reaction of Used Cooking Oil". *Al-Kimia: Jurnal Ilmu Kimia dan Terapan*. **8** (1): 83–92. 10.24252/al-kimia.v8i1.12173.

[14] R. Jenny, A. F. Suyadi, D. Auliardi, H. Devianto, and T. H. Soerawidjaja. (2021). "Karakterisasi Fotokatalis untuk Fotoreduksi Karbon Dioksida Menjadi Asam Format dalam Fasa Akuatik (Characterization of Photocatalysts for Photoreduction of Carbon Dioxide to Formic Acid in the Aqueous Phase)". *Indonesian Journal of Chemical Research*. **9** (2): 129–136. 10.30598/ijcr.2020.8-jen.

[15] O. Reyes, V. Rocío, M. Sánchez, A. José, E. García, and A. Cruz. (2025). "Green Synthesis of CaO-Fe3O4 Composites for Photocatalytic Degradation and Adsorption of Synthetic Dyes". *Environmental Science and Pollution Research*. **32** (15): 9901–9925. 10.1007/s11356-025-36310-w.

[16] D. S. Kumar, V. Sharma, J. Pradhan, S. Sharma, P. Singh, and J. Sharma. (2021). "Structural, Optical and Antibacterial Response of CaO Nanoparticles Synthesized via Direct Precipitation Technique". *Nano Biomedicine and Engineering*. **13** (2): 172–178. 10.5101/nbe.v13i2.p172-178.

[17] N. Nurhayati, M. Muhdarina, A. Linggawati, and S. S. Siregar. (2025). "Synthesis and Characterization of CaO-SiO2 Heterogeneous Catalyst of Blood Cockle Shells and Coconut Fiber Ash for Biodiesel Production from Crude Palm Oil". *Indonesian Journal of Chemistry*. **25** (4): 998–1011. 10.22146/ijc.91444.

[18] S. Guan, Y. Cheng, L. Hao, H. Yoshida, C. Tarashima, T. Zhan, T. Itoi, T. Qiu, and Y. Lu. (2023). "Oxygen Vacancies Induced Band Gap Narrowing for Efficient Visible-Light Response in Carbon-Doped TiO2". *Scientific Reports*. **13** (1): 14105. 10.1038/s41598-023-39523-6.

[19] R. Garg, R. Garg, N. O. Eddy, and M. I. Abdulraheem. (2025). "Green Synthesis of Calcium Oxide Nanocatalyst and Application in Transesterification of Waste Cooking Oil". *Bioresources and Bioprocessing*. **12** : 52. 10.1186/s40643-025-00879-4.

[20] S. Jähnigen, R. Vuilleumier, and A. Zehnacker. (2025). "The Genesis of OH-

Stretching Vibrational Circular Dichroism in Chiral Molecular Crystals". *Chemical Science*. **16** (22): 9833–9842. 10.1039/D4SC08055F.

[21] S. Ragab, M. R. Elkatory, M. A. Hassaan, and A. El Nemr. (2024). "Experimental, Predictive and RSM Studies of H2 Production Using Ag-La-CaTiO3 for Water-Splitting Under Visible Light". *Scientific Reports*. **14** (1): 1019. 10.1038/s41598-024-51219-z.

[22] E. Alsubhe. (2025). "One-Step Co-Precipitation Synthesis, Characterization, and Enhanced Photocatalytic Performance of CaO/TiO2-Supported γ-Al2O3 Nanocomposites (NCs) in Wastewater Treatment". *RSC Advances*. 24851–24861. 10.1039/D5RA03493K.

[23] P. T. Hue and H. T. Phuong. (2024). "Preparation and Characterization of Calcium Oxide from Snail Shell". *Journal of Science and Transport Technology*. **4** (3): 53–62. 10.58845/jstt.utt.2024.en.4.3.53-62.

[24] U. O. Bhagwat, M. C. Maridevaru, A. Al Souwaileh, J. J. Wu, and S. Anandan. (2024). "Anatase-Rutile Phase Transition of Ca@TiO2 Nanostructures for the Removal of Environmental Pollutants Under Visible Photon Illumination". *Inorganic Chemistry Communications*. **161** : 111987. 10.1016/j.inoche.2023.111987.

[25] D. W. Kurniawidi, S. Rahayu, A. Budianto, K. Saputra, W. P. Agista, T. Suprayogi, and R. Marlina. (2025). "Synthesis and Characterization of TiO2/CaTiO3 Perovskite Composite Derived from Pinctada maxima Shell Waste". *Science and Technology Indonesia*. **10** (3): 924–942. 10.26554/sti.2025.10.3.924-942.

[26] M. A. M. Shafiee and A. A. Jafari. (2017). "Co-Precipitation Synthesis of ZnO-TiO2 Nanostructure Composites for Arsenic Photodegradation from Industrial Wastewater". *International Journal of Environmental Science and Technology*. 10.1007/s13762-017-1585-7.

[27] A. V. Rane, K. Kanny, V. K. Abitha, and S. Thomas. (2018). In: "Synthesis of Inorganic Nanomaterials: Advances and Key Technologies". Elsevier Ltd. 121–139. 10.1016/B978-0-08-101975-7.00005-1.

[28] M. S. Lassoued, A. Lassoued, S. Ammar, A. Gadri, and A. Ben. (2018). "Synthesis and Characterization of Co-Doped Nano-TiO2 Through Co-Precipitation Method for Photocatalytic Activity". *Journal of Materials Science: Materials in Electronics*. 10.1007/s10854-018-8910-x.

[29] D. Y. Lee, J. Kim, J. Park, Y. Kim, I. Lee, M. Lee, and B. Kim. (2013). "Effect of Er Doping on Optical Band Gap Energy of TiO2 Thin Films Prepared by Spin Coating". *Current Applied Physics*. **13** (7): 1301–1305. 10.1016/j.cap.2013.03.025.

[30] B. Anitha and M. A. Khadar. (2020). "Anatase-Rutile Phase Transformation and Photocatalysis in Peroxide Gel Route Prepared TiO2 Nanocrystals: Role of Defect States". *Solid State Sciences*. **108** : 106392. 10.1016/j.solidstatesciences.2020.106392.

[31] M. Bonchio, J. Bonin, O. Ishitani, T. Lu, T. Morikawa, A. J. Morris, E. Reisner, D. Sarkar, F. M. Toma, and M. Robert. (2023). "Best Practices for Experiments and Reporting in Photocatalytic CO2 Reduction". *Nature Catalysis*. **6** (8): 657–665. 10.1038/s41929-023-00992-7.